Mechanism and Machine Theory 65 (2013) 14–28

Contents lists available at SciVerse ScienceDirect

Mechanism and Machine Theory

journal homepage: www.elsevier.com/locate/mechmt

A new method to design compliant mechanisms based on the inverse beam finite element model

Alejandro E. Albanesi, Martín A. Pucheta, Víctor D. Fachinotti *

Centro Internacional de Métodos Computacionales en Ingeniería (CIMEC-INTEC), Universidad Nacional del Litoral (UNL)/Consejo Nacional de Investigaciones Científicas y Técnicas (CONICET), Predio CCT-CONICET Santa Fe, Colectora Ruta Nacional 168, Paraje El Pozo, Santa Fe 3000, Argentina

ARTICLE INFO

Article history:
Received 5 July 2012
Received in revised form 18 February 2013
Accepted 25 February 2013
Available online xxxx

Keywords:
Inverse finite element method
Compliant mechanisms
Large elastic deformation
Medical devices

ABSTRACT

The motivation of this work is to introduce the inverse finite element method (IFEM) as a new method for the design of compliant mechanisms that must fit a prescribed shape after undergoing large elastic deformations under known service loads. This specific task is typical of a variety of mechanisms where the deformed shape and the responsible loads are known, while the problem is to determine the unloaded shape, i.e., the manufacturing shape of the mechanism.
The potentialities and the limitations of the IFEM are shown with three applications in the medical field: 1) a microgripper whose deformed shape is dictated by the object to hold; 2) a valve that must by-pass a prescribed flow rate when it is deformed under a prescribed pressure; and 3) a folder of an intra-ocular lens (IOL) whose deformed shape is determined by the optimal shape of the folded IOL.

1. Introduction

A compliant mechanism is a device that uses the compliance of its structure to achieve mechanical tasks such as force and motion transmission, and it relies on elastic strain in order to reach the desired degree of deformability [1].

Classically, the obtention of feasible configurations for flexible members that perform a mechanical task required the use of optimization techniques. The design variables are positions, characteristic dimensions and density of the members, among others. Common design objectives are the reduction of stress concentration, the reduction of volume or mass, the maximization of mechanical and geometrical advantages, and the attainment of a desired deformed shape.

According to the classical literature, the design of compliant mechanisms has been undertaken using optimization-based solvers aided by other methods such as the pseudo-rigid body model [1], the continuous material density parametrization [2,3], the ground structure parametrization [4], the load-path methods [5,6], the graph theory [7,8] or the level-set methods [9,10].

The process of solving any optimization problem consists of a series of steps (tens, hundreds, and even more), and at each one the governing equilibrium equations of the problem have to be solved.

In this work, we address the design of compliant mechanisms to accomplish a specific task: to attain an exact desired shape under the effect of service loads after large elastic deformations. The inverse finite element method (IFEM), for which the desired deformed shape is given, determines the undeformed shape of a mechanism by solving the equilibrium equations only once. The IFEM for two- and three-dimensional isotropic elastic bodies with known deformed shape and loads was originally proposed by Govindjee and Mihalic [11,12] and Yamada [13]. Recently, Fachinotti et al. [14] extended the IFEM for 3D orthotropic elastic material.

However, for a wide variety of compliant mechanisms that are properly modeled using beam elements [15,16], the use of 2D- or 3D solid finite elements entails a huge waste of computational resources. This motivated the formulation of the IFEM for elastic beams under large deformations, presented in Albanesi et al. [17].

* Corresponding author. Tel.: +54 342 4511594x1019; fax: +54 342 4511169.
E-mail addresses: aalbanes@santafe-conicet.gov.ar (A.E. Albanesi), mpucheta@intec.unl.edu.ar (M.A. Pucheta), vfachino@intec.unl.edu.ar (V.D. Fachinotti).
URL: http://www.cimec.org.ar (V.D. Fachinotti).

0094-114X/$ – see front matter © 2013 Elsevier Ltd. All rights reserved.
http://dx.doi.org/10.1016/j.mechmachtheory.2013.02.009

In this paper, we will illustrate the strengths and limitations of the beam-IFEM through applications to the design of biomedical tools and minimally invasive surgery (MIS) instruments. These applications are promising uses of compliant mechanisms since they eliminate wear debris, pinch points and lubrication, all of which are critical in the sensitive internal environment of the human body [18]. Three examples will be widely discussed: 1) a compliant microgripper, taking as reference the one proposed by Kohl et al. [19], 2) a compliant passive valve, following Seidemann et al. [20]; and 3) a folder for an intra-ocular-lens (IOL), based on that proposed by Erdman and Loftness [21].

2. Summary of the beam-IFEM

In this work, we aim to develop applications to compliant mechanisms of the inverse beam finite element introduced by Albanesi et al. [17]. For the sake of clarity, a self-contained summary is intended here.

2.1. Kinematics

Let $\mathcal{B}_0$ be the undeformed configuration of the beam with cross section $\mathcal{A}_0$ and length L_0, and S the coordinate along the neutral axis of $\mathcal{B}_0$, $0 < S < L_0$, as shown at the bottom of Fig. 1.

The position of any point $\mathbf{X} \in \mathcal{B}_0$ can be written as a function of S:

$$\mathbf{X}(S) = \mathbf{X}_0(S) + \mathbf{Y}(S) \tag{1}$$

where $\mathbf{X}_0$ is the trace of the neutral axis of $\mathcal{B}_0$ on the cross section $\mathcal{A}_0$ that contains $\mathbf{X}$, such that $\mathbf{Y} = \mathbf{X} - \mathbf{X}_0$ lies in $\mathcal{A}_0$.

Similarly, let $\mathcal{B}$ be the deformed configuration of such beam, with cross section $\mathcal{A}$ and length L, and s the coordinate along the neutral axis of $\mathcal{B}$, $0 < s < L$, as shown at the top of Fig. 1. The position of any point $\mathbf{x} \in \mathcal{B}$ can be expressed as:

$$\mathbf{x}(s) = \mathbf{x}_0(s) + \mathbf{y}(s) \tag{2}$$

where $\mathbf{x}_0$ is the trace of the neutral axis of $\mathcal{B}$ on the cross section $\mathcal{A}$ that contains $\mathbf{x}$, and $\mathbf{y} = \mathbf{x} - \mathbf{x}_0$ lies in $\mathcal{A}$.

Let us assume, as usual in the beam theory, that a cross-section does not deform and remains plane during deformation; however, if it is normal to the neutral axis at a given configuration, in general, it is not normal to the neutral axis at any other configuration due to shear effects. Then, the vectors $\mathbf{Y}$ and $\mathbf{y}$ in Eqs. (1) and (2) are related by the rotation law:

$$\mathbf{Y} = \mathbf{R}^T \mathbf{y} \tag{3}$$

where $\mathbf{R}$ is a proper orthogonal matrix, i.e. $\mathbf{R}^T = \mathbf{R}^{-1}$ and $\det(\mathbf{R}) = +1$.

The matrix $\mathbf{R}$ is completely determined by its rotation vector ψ by means of Rodrigues' formula:

$$\mathbf{R}(\psi) = \mathbf{I} + \frac{\sin\|\psi\|}{\|\psi\|}\,\tilde{\psi} + \frac{1-\cos\|\psi\|}{\|\psi\|^2}\,\tilde{\psi}\,\tilde{\psi} \tag{4}$$

where $\mathbf{I}$ is the identity matrix and $\tilde{\psi}$ is the skew-symmetric matrix associated to vector ψ, such that $\tilde{\psi}\mathbf{a} = \psi \times \mathbf{a}$ for any vector $\mathbf{a}$.

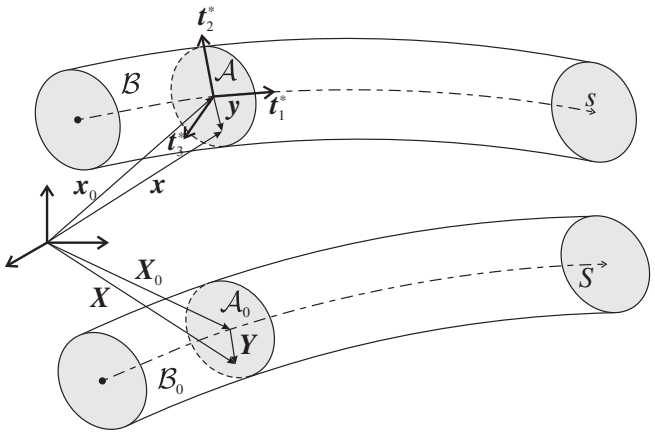

Fig. 1. Undeformed (bottom) and deformed configuration of the beam.

Using the IFEM, the vector fields $\mathbf{x}_0$ and $\mathbf{y}$ that determine the position of any point $\mathbf{x} \in \mathcal{B}$ are assumed to be known. The IFEM problem consists of finding the vector field $\mathbf{X}_0$ and the tensor field $\mathbf{R}$ in order to completely define the position of any point $\mathbf{X} \in \mathcal{B}_0$. However, since the vector field ψ suffices to completely describe the rotation $\mathbf{R}$, the unknown fields for the IFEM are finally the vector fields $\mathbf{X}_0$ and ψ.

2.2. Equilibrium equations

Let $\mathbf{t}$ be the traction vector field per unit area of $\mathcal{A}$. The resultant force $\mathbf{n}$ and the resultant moment $\mathbf{m}$ with respect to $\mathbf{x}_0$ of the traction vector $\mathbf{t}$ acting throughout $\mathcal{A}$, the so-called internal efforts, are:

$$\mathbf{n} = \int_{\mathcal{A}} \mathbf{t} \; \mathrm{d}s \tag{5}$$

$$\mathbf{m} = \int_{\mathcal{A}} (\mathbf{x} - \mathbf{x}_0) \times \mathbf{t} \; \mathrm{d}s. \tag{6}$$

Let $\mathbf{b}$ be the (given) vector of body loads per unit length of the beam. We call external efforts the resultant force $\mathbf{n}_{\mathrm{ext}}$ and the resultant moment $\mathbf{m}_{\mathrm{ext}}$ with respect to $\mathbf{x}_0$ of the body loads $\mathbf{b}$ acting throughout $\mathcal{A}$:

$$\mathbf{n}_{\mathrm{ext}} = \int_{\mathcal{A}} \mathbf{b} \; \mathrm{d}s \tag{7}$$

$$\mathbf{n}_{\mathrm{ext}} = \int_{\mathcal{A}} (\mathbf{x} - \mathbf{x}_0) \times \mathbf{b} \; \mathrm{d}s. \tag{8}$$

Now, the translation and rotation equilibrium equations at any point $\mathbf{x} \in \mathcal{B}$ can be expressed respectively as

$$\mathbf{n}' + \mathbf{n}_{\mathrm{ext}} = 0 \tag{9}$$

$$\mathbf{m}' + \mathbf{x}'_0 \times \mathbf{n} + \mathbf{m}_{\mathrm{ext}} = 0 \tag{10}$$

where $(*)' \equiv \mathrm{d}(*)/\mathrm{d}s$ and 0 denotes the null vector.

The unknown undeformed configuration $\mathcal{B}_0$ is completely determined by the material position field $\mathbf{X}$. In its turn, under the assumptions of beam theory, $\mathbf{X}$ is completely determined by the neutral-axis material position field $\mathbf{X}_0$ and the rotation vector field ψ. Then, the weak form of equilibrium Eqs. (9) and (10) takes the form: to find the vector fields $\mathbf{X}_0$ and ψ such that

$$\int_{\mathcal{B}} \left\{ \mathbf{n} \cdot \left[(\delta \mathbf{X}_0)' + \mathbf{x}'_0 \times \delta\psi \right] + \mathbf{m} \cdot (\delta\psi)' \right\} \mathrm{d}s = \int_{\mathcal{B}} (\mathbf{n}_{\mathrm{ext}} \cdot \delta \mathbf{X}_0 + \mathbf{m}_{\mathrm{ext}} \cdot \delta\psi) \mathrm{d}s \tag{11}$$

for all admissible variations $\delta\mathbf{X}_0$ and $\delta\psi$.

2.3. Deformation

In beam theory, the deformation is measured by the vectors Γ and $\mathbf{K}$ describing respectively the strain and the curvature of the neutral axis, given as

$$\Gamma = \mathbf{R}^T \frac{\mathrm{d}\mathbf{x}_0}{\mathrm{d}S} - \frac{\mathrm{d}\mathbf{X}_0}{\mathrm{d}S} \tag{12}$$

$$\mathbf{K} = \mathbf{T} \frac{\mathrm{d}\psi}{\mathrm{d}S} \tag{13}$$

where $\mathbf{T}$ is the tangent operator

$$\mathbf{T}(\psi) = \mathbf{I} + \frac{cos\|\psi\| - 1}{\|\psi\|^2} \tilde{\psi} + \frac{1}{\|\psi\|^2} \left(1 - \frac{sin\|\psi\|}{\|\psi\|} \right) \tilde{\psi} \, \tilde{\psi}. \tag{14}$$

Note that Γ and $\mathbf{K}$ are material measures of deformation. In the IFEM, we use their spatial counterparts:

$$\gamma = \mathbf{R}\Gamma = \frac{1}{S'} (\mathbf{x}'_0 - \mathbf{R}\mathbf{X}'_0) \tag{15}$$

$$\kappa = \mathbf{R}\mathbf{K} = \frac{1}{S'} \mathbf{R}\mathbf{T}\psi'. \tag{16}$$

2.4. Material behavior

Let us assume that the material obeys the following linear-elastic constitutive laws

$$\mathbf{n} = \mathbf{C}^{\mathrm{n}}\gamma \tag{17}$$

$$\mathbf{m} = \mathbf{C}^{\mathrm{m}}\kappa \tag{18}$$

with

$$\mathbf{C}^{\mathrm{n}} = EA\mathbf{t}_1^*\otimes\mathbf{t}_1^* + GA_2\mathbf{t}_2^*\otimes\mathbf{t}_2^* + GA_3\mathbf{t}_3^*\otimes\mathbf{t}_3^* \tag{19}$$

$$\mathbf{C}^{\mathrm{m}} = GJ\mathbf{t}_1^*\otimes\mathbf{t}_1^* + EI_2\mathbf{t}_2^*\otimes\mathbf{t}_2^* + EI_3\mathbf{t}_3^*\otimes\mathbf{t}_3^* \tag{20}$$

where E and G are the material Young and shear moduli, respectively, $\mathbf{t}_1^* \equiv \mathbf{x}_0'$ is the unit vector along the axis of the deformed beam $\mathcal{B}$, $\mathbf{t}_2^*$ and $\mathbf{t}_3^*$ are the unit vectors along the principal axis of the deformed section $\mathcal{A}$ (see Fig. 1), A is the area of $\mathcal{A}$, A_2 and A_3 are the shear areas in the direction of $\mathbf{t}_2^*$ and $\mathbf{t}_3^*$, respectively, I_2 and I_3 are the rotational moment of inertia of $\mathcal{A}$ with respect to $\mathbf{t}_2^*$ and $\mathbf{t}_3^*$, respectively, and J is the torsional moment of inertia of $\mathcal{A}$. For the IFEM, all these mechanical and geometrical properties are assumed to be known.

Using beam theory, the Cauchy stress tensor σ can be determined in terms of the internal efforts $\mathbf{n}$ and $\mathbf{m}$ and the geometric characteristics of the cross section. This way of computing σ gives rise to a huge number of formulas regarding the huge number of commonly used cross section geometries, as shown in the classical book of Timoshenko and Goodier [22], which presents formulas for elliptical solid and hollow sections, narrow and normal rectangular sections, rolled-profile sections, etc. For instance, in a beam with rectangular cross section $A = b_1 b_2$ (b_i stands for the dimension along the axis $\mathbf{t}_i^*$) deforming in the plane normal to t_2^*, the non-zero components of the Cauchy stress are

$$\sigma_{11} = \frac{n_1}{A} + \frac{m_2}{I_2}y_3 \tag{21}$$

$$\sigma_{13} = \sigma_{31} = \frac{n_3}{A_3} \tag{22}$$

where $I_2 = b_2 b_3^3/12$ and $A_3 = 5A/6$.

2.5. Finite element formulation

A general beam structure is an assemblage of several beams with curved neutral axis and variable cross section. Let us approximate each beam as one or more straight beams, each one having a constant cross section. Each straight beam constitutes a beam finite element.

Let $\mathcal{B}$ be the known deformed configuration of the whole structure, which is divided into N beam finite elements $\mathcal{B}^e$.

The current *inverse* beam element $\mathcal{B}^e$ is a straight, mixed linear-linear finite element having two nodes located at its ends, whose *direct* counterpart is the finite element proposed by Cardona and Géradin [23].

By *mixed linear–linear*, we mean that there are two unknown fields, $\mathbf{X}_0$ and ψ, and they are both linearly interpolated inside the element $\mathcal{B}^e$, i.e.:

$$\mathbf{X}_0(s) = \varphi_1(s)\mathbf{X}_{0_1} + \varphi_2(s)\mathbf{X}_{0_2} \tag{23}$$

$$\psi_0(s) = \varphi_1(s)\psi_1 + \varphi_2(s)\psi_2 \tag{24}$$

where $(*)_i$ is the value of $(*)$ at node $i = 1, 2$, and $\varphi_i(s)$ is the linear shape function associated to node i. If node 1 is that located at $s = 0$ and node 2 is that located at $s = L^e$, with L^e being the length of the neutral axis of element $\mathcal{B}^e$, we have

$$\varphi_1(s) = 1 - \frac{s}{L^e} \equiv 1 - \varphi_2(s) \tag{25}$$

2.6. Equilibrium equations for IFEM

The equilibrium equations for the IFEM are obtained by using the standard Galerkin procedure [24]: the unknowns fields $\mathbf{X}_0$ and ψ as well as their variations $\delta\mathbf{X}_0$ and $\delta\psi$ are approximated as defined by Eqs. (23) and (24). Doing this, the equilibrium equations given in weak form by Eq. (11), restricted to the element $\mathcal{B}^e$, take the form:

$$\mathbf{F}_{\mathrm{int}}^e - \mathbf{F}_{\mathrm{ext}}^e = 0 \tag{26}$$

where $\mathbf{F}^e_{\text{int}}$ and $\mathbf{F}^e_{\text{ext}}$ are respectively the vectors of internal and external forces of the element $\mathcal{B}^e$, given by

$$\mathbf{F}^e_{\text{int}} = \int_{\mathcal{B}^e} \mathbf{B}^T \begin{bmatrix} \mathbf{n} \\ \mathbf{m} \end{bmatrix} \mathrm{d}s \tag{27}$$

$$\mathbf{F}^e_{\text{ext}} = \int_{\mathcal{B}^e} \varphi^T \begin{bmatrix} \mathbf{n}_{ext} \\ \mathbf{m}_{ext} \end{bmatrix} \mathrm{d}s \tag{28}$$

with

$$\mathbf{B} = \begin{bmatrix} \varphi_1'\mathbf{I} & \varphi_1(\widetilde{\mathbf{x}_0'}) & \varphi_2'\mathbf{I} & \varphi_2(\widetilde{\mathbf{x}_0'}) \\ \mathbf{O} & \varphi_1'\mathbf{I} & \mathbf{O} & \varphi_2'\mathbf{I} \end{bmatrix} \tag{29}$$

$$\varphi = \begin{bmatrix} \varphi_1\mathbf{I} & \mathbf{O} & \varphi_2\mathbf{I} & \mathbf{O} \\ \mathbf{O} & \varphi_1\mathbf{I} & \mathbf{O} & \varphi_2\mathbf{I} \end{bmatrix} \tag{30}$$

where $\mathbf{O}$ is the null matrix.

Once we have computed the vector of internal and external forces of all the elements $\mathcal{B}^e$, $e = 1, \ldots, N$, they are assembled in the global vectors

$$\mathbf{F}_{\text{int}} = \sum_{e=1}^{N} \mathbf{F}^e_{\text{int}} \tag{31}$$

$$\mathbf{F}_{\text{ext}} = \sum_{e=1}^{N} \mathbf{F}^e_{\text{int}}. \tag{32}$$

For further details on the assemblage process, we refer to any classical book on FEM (e.g., [24]).

After assemblage of both terms in Eq. (26), we obtain the equilibrium equation for the whole structure $\mathcal{B}$:

$$\mathbf{F}_{\text{res}} \equiv \mathbf{F}_{\text{int}} - \mathbf{F}_{\text{ext}} = 0 \tag{33}$$

This is a non-linear discrete system of equations, whose unknowns are the values of $\mathbf{X}_0$ and ψ at all the nodes $i = 1 \ldots, M$ of the whole beam structure $\mathcal{B}$, which are grouped in the global unknown vector

$$\mathbf{Q} = \begin{bmatrix} \mathbf{X}_{0_1} \\ \psi_1 \\ \vdots \\ \mathbf{X}_{0_M} \\ \psi_M \end{bmatrix}. \tag{34}$$

We remark that the equilibrium Eq. (33) governing the IFEM is identical to those that govern the *direct* FEM, except that the unknowns and the given data are interchanged.

The non-linear Eq. (33) is solved iteratively using the Newton–Raphson method [25]. The process starts (i.e., at iteration $k = 0$) by assuming an initial guess $\mathbf{Q}^{(0)}$. At a generic iteration $k > 0$, once $\mathbf{Q}^{(k-1)}$ is known, we compute $\mathbf{Q}^{(k)}$ by solving the linear system:

$$\mathbf{F}_{\text{res}}\left(\mathbf{Q}^{(k-1)}\right) + \mathbf{S}\left(\mathbf{Q}^{(k-1)}\right)\left(\mathbf{Q}^{(k)} - \mathbf{Q}^{(k-1)}\right) = 0 \tag{35}$$

where $\mathbf{S}$ is the tangent stiffness matrix, defined as

$$\mathbf{S} = \frac{\mathrm{d}\mathbf{F}_{\text{res}}}{\mathrm{d}\mathbf{Q}}. \tag{36}$$

The process finishes when $\|\mathbf{F}_{\text{res}}(\mathbf{Q}^{(k)})\|$ is less than a small real positive value, the so-called tolerance ϵ. Generally, the Newton–Raphson scheme guarantees the fastest convergence to the solution, i.e., makes $\|\mathbf{F}_{\text{res}}(Q^{(k)})\| < \epsilon$ for a lower k than any other method. For a detailed description of the computation of $\mathbf{F}_{\text{int}}$, $\mathbf{F}_{\text{ext}}$ and $\mathbf{S}$, the interested reader is referred to the work of Albanesi et al. [17], where the beam-IFEM was originally proposed.

Concerning the implementation, the beam-IFEM was coded in GNU Octave [26] under a Linux platform.

3. IFEM for the design of compliant mechanisms

In this section, the use of the IFEM for the design of compliant mechanisms to exactly fit a desired shape after large elastic deformations will be illustrated. The problem to be solved can be stated as follows: to determine the manufacturing shape of the compliant mechanism assuming that we know:

1. the deformed configuration $\mathcal{B}$ of the mechanism;
2. the way the mechanism is supported;
3. the way the mechanism is actuated;
4. the properties of the material used to build the mechanism.

3.1. Feasibility of the IFEM solution

Given the above data, the IFEM gives us the undeformed configuration $\mathcal{B}$. But, in order to identify $\mathcal{B}$ with the manufacturing shape, the following tests must be succeeded:

1. Mechanical tests:
   (a) Validity of the hypothesis of elastic material behavior, as assessed using the yield criterion best-suited for the employed material. For instance, according to the widely used von-Mises yield criterion, a beam remains elastic if the Cauchy stress tensor throughout the volume of the beam satisfies

$$\sqrt{\sigma_{11}^2 + 3(\sigma_{12}^2 + \sigma_{13}^2)} < \sigma_Y$$

   where the l.h.s. defines the von-Mises equivalent stress and σ_Y is the yield strength of the material.
   (b) Uniqueness of the solution, which is lost when an unstable equilibrium state (or *critical point*) is met during deformation. The expertise of the designer frequently suffices to detect the occurrence of critical points. In case of doubt, this can be formally assessed by using the spectrum test [27].
2. Topological tests:
   (a) Absence of interpenetrated beam elements: the IFEM solution may exhibit beam elements penetrating or crossing each other.
   (b) Sometimes, the mechanism is required to keep inside a *design domain* along the entire deformation.
   A simple ocular inspection is enough to assess the fulfillment of topological tests.

In general, mechanical and topological tests also apply to the configurations corresponding to intermediate load steps.

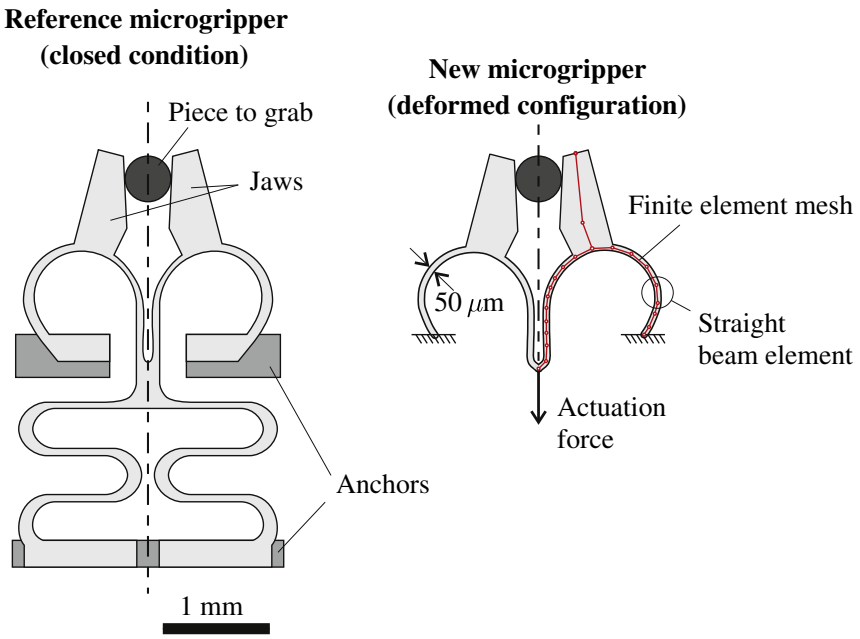

Fig. 2. Compliant microgripper proposed by Kohl et al. [19] in its closed condition (on the left) and deformed configuration of the new microgripper.

Table 1
Properties of the proposed microgripper.

Section of flexible beams	$A = 2500\ \mu m^2$ (square, constant)
Actuation force	$P = 40$ mN
Material	Stainless spring steel
Young modulus	$E = 200$ GPa
Shear modulus	$G = 76.9$ GPa
Yield strength	$\sigma_Y = 1$ GPa

3.2. Design of a microgripper

Let us use the IFEM to design a compliant microgripper to perform the same task as that of Kohl et al. [19], depicted on the left of Fig. 2. This task is actually conditioning the deformed configuration of the microgripper, which represents the microgripper grabbing a given object. Here is the major advantage of IFEM: the designer can define the exact deformed configuration of the microgripper such that a geometrically-complex fragile piece can be carefully grabbed.

The undeformed shape of the new microgripper is determined assuming the following as given data:

1. The deformed configuration $\mathcal{B}$, composed of the jaws attached to two flexible circular beams, as shown on the right of Fig. 2. The jaws as well as the neutral axis of the flexible beams coincide with those of Kohl et al.'s microgripper. However, unlike Kohl et al., the flexible beams are assumed to have constant 50 μm-side square cross section.
2. The circular beams are assumed to be clamped at their ends, like those in Kohl et al.'s microgripper.
3. The new microgripper is assumed to be actuated by applying a force $P = 40$ mN at its midpoint, pointing downwards along the symmetry axis, as shown on the right side of Fig. 2. The prescribed force can be produced by an electro-thermal actuator (like in Kohl et al.'s microgripper), an electro-magnetic actuator [28], a piezo-electric actuator [29], etc.
4. Instead of the shape memory alloy used by Kohl et al., the new microgripper is assumed to be made of stainless spring steel.

Due to the symmetry of the deformed configuration and the supports with respect to the direction of the actuating force, only one half of the mechanism is modeled. The whole finite element mesh consists of 42 straight beam elements, and is finer where the neutral axis is more curved or when higher stress gradients along the neutral axis are expected.

Table 1 summarizes the data used for modeling the new microgripper.

Fig. 3 shows the IFEM solution of this problem, i.e., the undeformed configuration $\mathcal{B}_0$ of a mechanism that *should* take the desired shape $\mathcal{B}$ after actuation. However, as mentioned in Section 1, in order to assimilate $\mathcal{B}_0$ to the manufacturing shape of the microgripper, we must verify that:

1. The material remains elastic along the entire deformation, which is confirmed by Fig. 4: the maximal von-Mises stress – occurring at the clamped section – attains 0.69 GPa, that is sufficiently lower than the yield strength of the spring steel used to fabricate the mechanism (1 GPa).
2. The deformation path is free of critical points, as it is evident to the naked eye (and can be further formally confirmed by using the spectrum test [27]).
3. Absence of interpenetrated beam elements, as easily confirmed by ocular inspection.

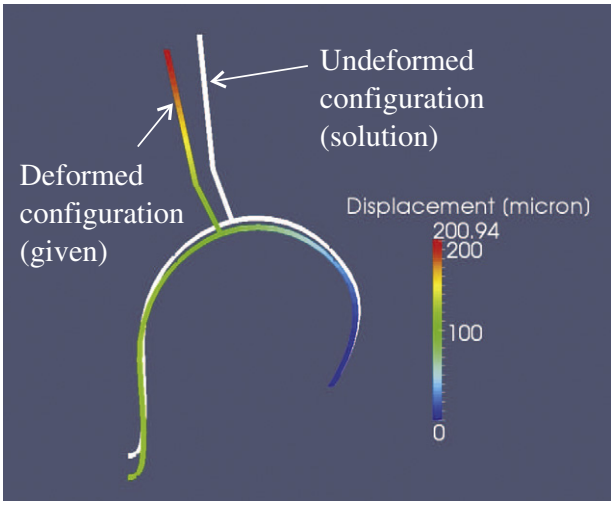

Fig. 3. IFEM solution for the new microgripper. The color bar gives the magnitude of the displacement. (For interpretation of the references to color in this figure legend, the reader is referred to the web version of this article.)

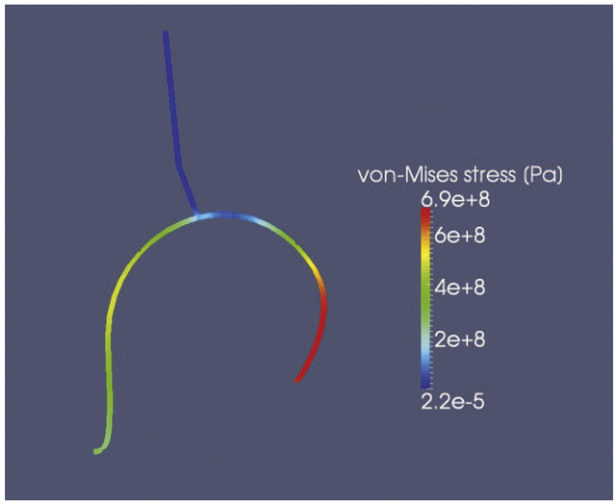

Fig. 4. Maximal value of the von-Mises stress within the cross section all along the new microgripper, to be compared with the yield strength of stainless spring steel (1 GPa).

Having succeeded all these tests, the IFEM-computed undeformed configuration $\mathcal{B}_0$ actually constitutes the manufacturing shape of the microgripper.

As mentioned above, the current IFEM has as its *direct* counterpart the FEM for beams proposed by Cardona and Géradin [23]. Then, let us solve the corresponding *direct* FEM problem to find the deformed configuration for the IFEM-computed undeformed configuration of the microgripper for the same given supports and actuation. The difference between the nodal positions in the deformed mesh given as data for IFEM and those in the deformed mesh recovered as solution of FEM, plotted in Fig. 5, gives us an idea of the accuracy of the current IFEM compared to a widely used and validated FEM. Considering that it accounts for just 0.07% of the maximal displacement shown in Fig. 3, this error is negligible.

3.3. Design of a passive microvalve

The second application of the IFEM concerns the design of a passive microvalve whose task is identical to that of the microvalve proposed by Seidemann et al. [20], depicted in Fig. 6. Integrated to a microchannel with thickness 360 μm and width 200 μm, the valve must close the channel when the pressure drop attains a prescribed value Δp, and bypass a specified flow when the pressure drop vanishes.

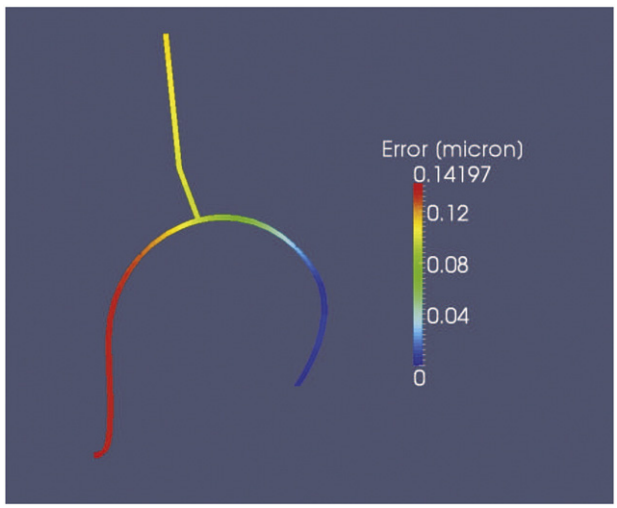

Fig. 5. Magnitude of the difference between the nodal positions in the deformed mesh given as data for IFEM and those in the deformed mesh recovered as solution of FEM.

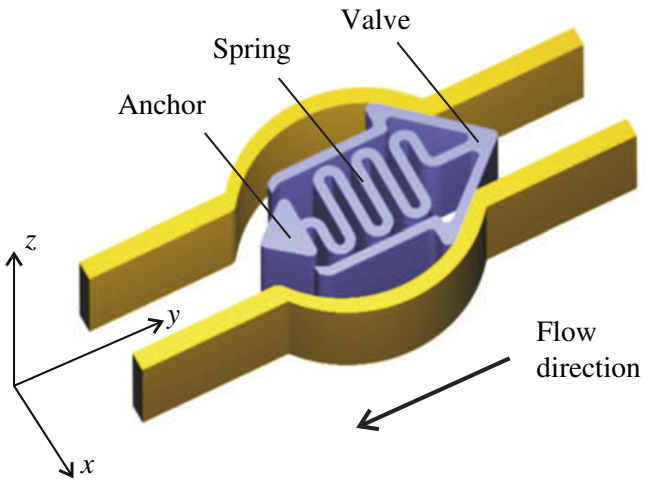

Fig. 6. Compliant passive valve to seal a microchannel proposed by Seidemann et al. [20].

The first step in seeking the manufacturing shape of the current microvalve is to solve the IFEM problem of determining the undeformed configuration $\mathcal{B}_0$, assuming that:

1. The deformed configuration $\mathcal{B}$ of the valve, which corresponds to its closed position, is known. As a first approach, we take as reference the configuration of Seidemann et al.'s mechanism (valve, spring, anchor) in closed condition, schematized in Fig. 7. The valve itself is assumed to be rigid. The spring is assumed to have constant rectangular cross section with height (in-plane) $b_2 = 6$ μm and width (out-of-plane) $b_3 = 11$ μm. The finite element mesh of the whole mechanism consists of 88 straight beam elements, and is finer where the neutral axis is more curved or where higher stress gradients along the neutral axis are expected.
2. The current mechanism is clamped at the anchor, identical to that of Seidemann et al.
3. The valve must close under a given pressure drop Δp. This pressure drop was not specified by Seidemann et al. Let us assume $\Delta p = 1$ kPa, which defines the current microvalve as a low-pressure one [30]. The resultant of Δp is a force actuating along the axis of the channel (y-axis in Fig. 7).
4. Like that of Seidemann et al., the new valve is made of the monomer SU8.

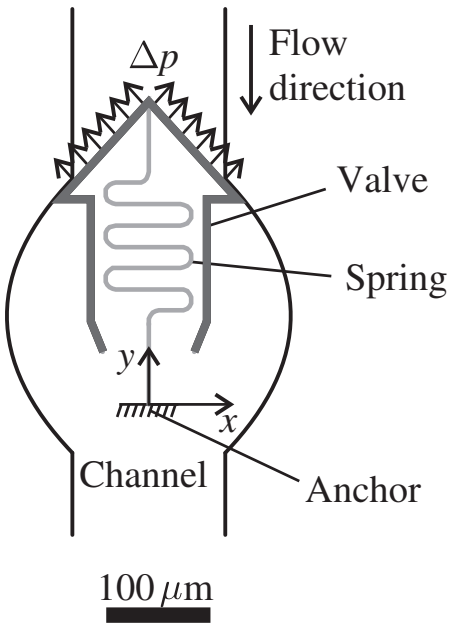

Fig. 7. Closed (deformed, given) configuration of the microvalve under a prescribed pressure drop Δp, inspired in the design of Seidemann et al. [20].

Table 2
Properties of the proposed microvalve.

Section of the spring	Rectangular, constant
Height (in-plane)	$b_2 = 6$ μm
Width (out-of-plane)	$b_3 = 11$ μm
Pressure drop for closing	$\Delta p = 1$ kPa
Axial displacement of the valve	$u_y = 50 \pm 2$ μm
Material	SU8
Young modulus	$E = 3.2$ GPa
Shear modulus	$G = 1.3$ GPa
Yield strength	$\sigma_Y = 73$ MPa

Table 2 summarizes the data used for modeling the new microvalve.

There is an additional design requirement that is not satisfied a priori by IFEM since it involves the valve in its open (i.e., undeformed) condition: a certain sealing gap is needed, depending on the prescribed flow to by-pass. Since this was not specified by Seidemann et al., let us assume that the desired opening is attained when axial displacement of the valve is $u_y = 50 \pm 2$ μm. In fact, the cross section of the spring was chosen to satisfy this condition.

Fig. 8 shows the IFEM-computed undeformed configuration, which actually attains the desired opening. However, two topological defects are observed:

1. The spring is penetrating the valve. Since the penetration depth is about one tenth of the height of the beam, this defect should be easily overcome by slightly modifying the shape of the spring and/or its cross section.
2. The displacement of the valve is not centered with respect to the axis of the channel due to the lack of symmetry of the spring with respect to the axis of the channel. The eccentric (undesired) displacement u_x is about one-third of the axial (desired) displacement u_y.

Note that the valve designed by Seidemann et al. – although they claimed the contrary – cannot remain centered during deformation because its flexible spring is non-symmetric with respect to the direction of the pressure resultant. Without information about the pressure drop and the sealing gap, it is not possible to assess how critical this defect is for the design of Seidemann et al.

To avoid eccentricity, we propose to replace the unique non-symmetric spring by two springs arranged symmetrically with respect to the axis, as shown in Fig. 9. In order to achieve a similar opening as before, the cross section of each spring, still constant and rectangular, has height (in-plane) $b_2 = 3$ μm and width (out-of-plane) $b_3 = 7$ μm.

In this case, given the symmetry of the deformed configuration and the supports with respect to the actuating force, only one half of the mechanism is modeled. The finite element mesh of this part of the mechanism consists of 84 straight beam elements, and is finer where the neutral axis is more curved or higher stress gradients along the neutral axis are expected.

Fig. 10 shows the corresponding undeformed configuration computed by the IFEM, which is, now, free of topological defects.

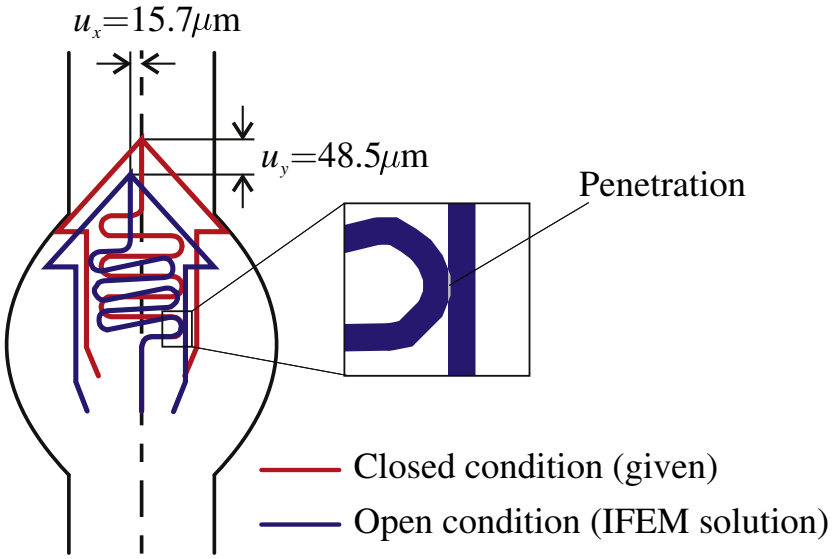

Fig. 8. IFEM solution for the microvalve with non-symmetric spring.

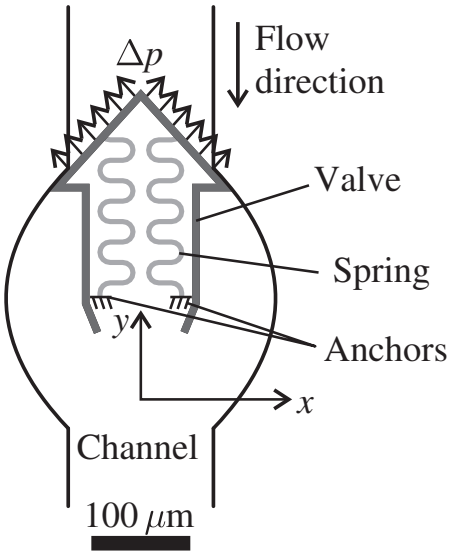

Fig. 9. Microvalve with two springs arranged symmetrically with respect to the axis of the channel, shown in its closed (deformed, known) configuration under a prescribed pressure drop Δp.

The feasibility of the solution regarding the mechanical tests of Section 3.1 remains to be checked:

1. The absence of critical points, evident for an experienced designer in this case, can be confirmed by using the spectrum test [27].
2. Assuming the von-Mises yield criterion to hold, the validity of the elastic hypothesis is confirmed after comparing the von-Mises stress plotted in Fig. 11 with the yield strength of SU8 (73 MPa).

3.4. Design of an IOL folding device

An intraocular lens (IOL) is a replacement lens that is implanted into the eye after the removal of part of the natural lens in cataract surgery. Fig. 12 shows the rigid four-bar mechanism to fold a soft IOL proposed by Erdman and Loftness [21]. When this mechanism is actuated, the lens adopts a σ-shape such that it can be delivered into the eye through a small incision.

As alternative to the Erdman and Loftness's rigid planar mechanism, we propose the compliant three-dimensional mechanism depicted in Fig. 13. It is designed in order to closely match the desired (three-dimensional) σ-shape of the folded IOL when deformed. In its deformed configuration, the whole folder fits a box having 5 mm in the x-direction, 2.45 mm in the y-direction and 4.25 mm in the z-direction, while the diameter of the unfolded IOL is 6 mm. The IFEM model is depicted in Fig. 14: all the beams are assumed to have 0.1 mm-side square cross sections, the actuation consists of three forces of magnitude $P = 8$ mN pointing in the $-$ y-direction, and the mechanism is hinged to the ground at six points.

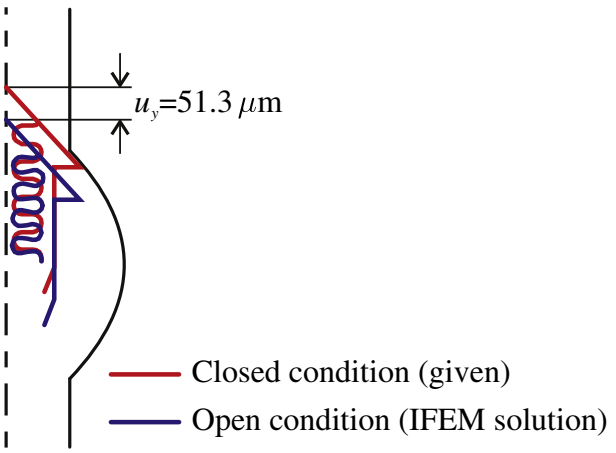

Fig. 10. IFEM solution for the symmetric microvalve.

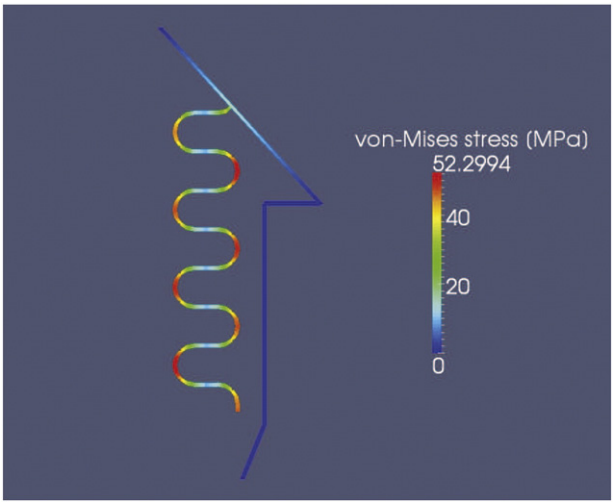

Fig. 11. Von-Mises equivalent stress for the symmetric microvalve, to be compared with the yield strength of SU8 (73 MPa).

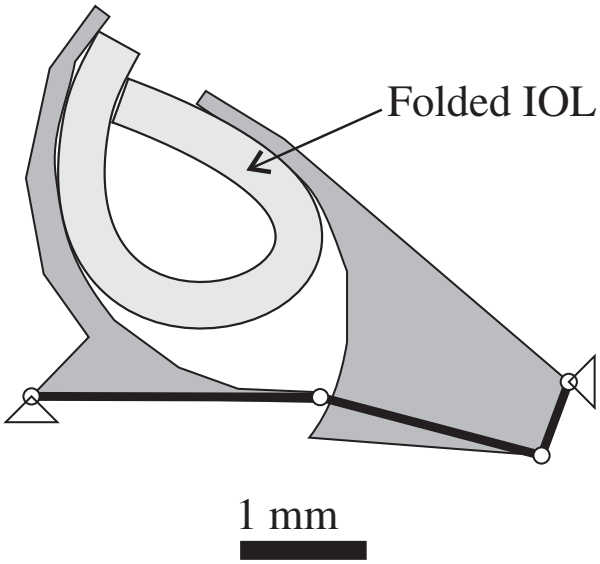

Fig. 12. Rigid four-bar linkage for folding an IOL into a σ-shape, proposed by Erdman and Loftness [21].

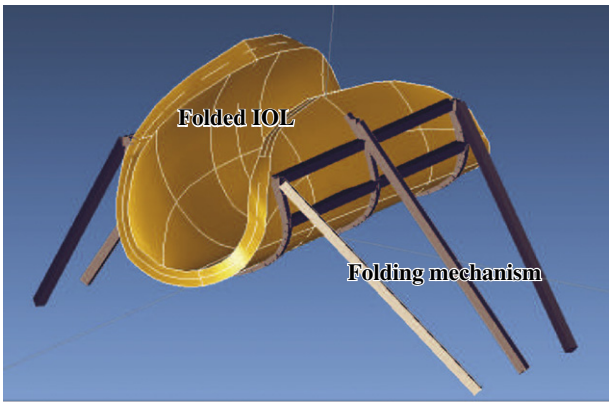

Fig. 13. Proposed compliant three-dimensional device for folding an IOL into a desired shape.

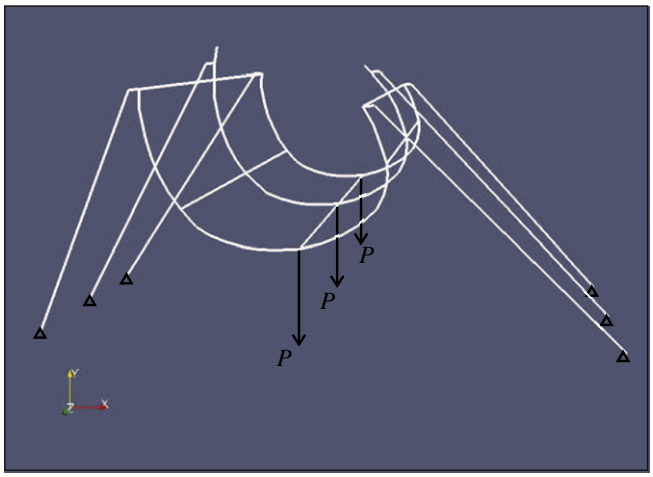

Fig. 14. Model of the compliant three-dimensional IOL folder in its deformed configuration.

The finite element mesh of the whole mechanism consists of 207 straight beam elements, and is denser where the neutral axis is more curved or higher stress gradients along the neutral axis are expected.

Further, the proposed mechanism is assumed to be made of polypropylene.

Table 3 lists the data used for modeling this compliant IOL folder.

Given the deformed configuration, the supports and the actuation forces, we use IFEM to compute the undeformed configuration, shown in Fig. 15.

Fig. 16 shows the maximal von-Mises stresses developed in the proposed mechanism, which are lower than the yield strength of polypropylene (43 MPa) throughout the mechanism. Hence, according to the von-Mises yield criterion, the hypothesis of elastic material behavior is verified.

Further, we do not find interpenetrated beams nor critical points along the deformation path of the proposed mechanisms.

Finally, it can be said that IFEM has given us the manufacturing shape of the new IOL folder, which is actually that of the undeformed configuration shown in Fig. 15.

Table 3
Properties of the proposed IOL folder.

Section of the all the beams	$A = 0.01\ \text{mm}^2$ (square, constant)
Actuation force	3×8 mN
Material	Polypropylene
Young modulus	$E = 1.4$ GPa
Shear modulus	$G = 0.48$ GPa
Yield strength	$\sigma_Y = 43$ MPa

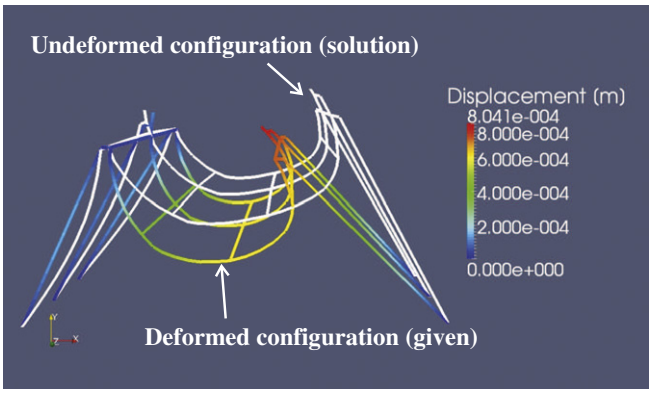

Fig. 15. IFEM solution for the compliant three-dimensional IOL folder. The color bar gives the magnitude of the displacement. (For interpretation of the references to color in this figure legend, the reader is referred to the web version of this article.)

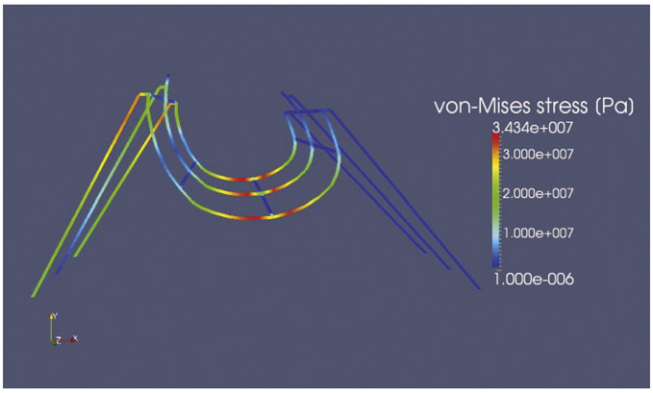

Fig. 16. Maximal von-Mises equivalent stresses throughout the compliant three-dimensional IOL folder, to be compared with the yield strength of polypropylene (43 MPa).

4. Conclusions

This paper introduced the use of the beam-IFEM for the design of compliant mechanisms to exactly fit a specified shape after large elastic deformations. IFEM determines the undeformed configuration of the mechanism by solving the non-linear equilibrium equation only once, unlike classical methods based on optimization techniques, which have to solve similar equations tens, hundreds, and even more times.

The IFEM-computed undeformed configuration has to pass some tests to become an admissible manufacturing shape: the validity of the elastic hypothesis, the absence of points of unstable equilibrium, the absence of interpenetrated beams, and to keep into a design domain. At the present state of development, IFEM is not capable of satisfying these requirements automatically.

Three successful applications in the field of medical devices were detailed: a microgripper, a microvalve, and a lens folding device. They served to illustrate the potential of IFEM to design new devices and improve existing ones.

Acknowledgments

The authors gratefully acknowledge the financial support from CONICET (Argentine Council for Scientific and Technical Research) and UNL (National University of Littoral, Santa Fe, Argentina) via their respective research programs.

References

[1] L.L. Howell, Compliant Mechanisms, John Wiley & Sons, 2001.
[2] N. Kikuchi, M.P. Bendsøe, Generating optimal topologies in structural design using a homogenization method, Computer Methods in Applied Mechanics and Engineering 71 (1988) 197–224.
[3] M.P. Bendsøe, Optimal shape design as a material distribution problem, Structural and Multidisciplinary Optimization 1 (1989) 193–202.
[4] M.I. Frecker, G.K. Ananthasuresh, S. Nishiwaki, N. Kikuchi, S. Kota, Topological synthesis of compliant mechanisms using multi-criteria optimisation, ASME Journal of Mechanical Design 119 (1997) 238–245.
[5] K.J. Lu, S. Kota, Design of compliant mechanisms for morphing structural shapes, Journal of Intelligent Systems and Structures 14 (2003) 379–391.
[6] K.J. Lu, S. Kota, An effective method of synthesizing compliant adaptive structures using load path representation, Journal of Intelligent Systems and Structures 16 (2005) 307–317.
[7] H. Zhou, K.-L. Ting, Topological synthesis of compliant mechanisns using spanning tree theory, ASME Journal of Mechanical Design 127 (2005) 753–759.
[8] M.A. Pucheta, A. Cardona, Design of bistable compliant mechanisms using precision-position and rigid-body replacement methods, Mechanism and Machine Theory 45 (2010) 304–326.
[9] Y.M. Wang, S. Chen, X. Wang, Y. Mei, Design of multi-material compliant mechanisms using level set methods, ASME Journal of Mechanical Design 5 (2005) 941–956.
[10] P. Wei, Y.M. Wang, Parametric structural shape and topology optimization method with radial basis functions and level-set method, Proceedings of ASME International Design Engineering Technical Conferences & Computers and Information in Engineering Conference (IDETC/CIE2006), Philadelphia, Pennsylvania, USA, 2006.
[11] S. Govindjee, P.A. Mihalic, Computational methods for inverse finite elastostatics, Computer Methods in Applied Mechanics and Engineering 136 (1996) 47–57.
[12] S. Govindjee, P.A. Mihalic, Computational methods for inverse deformations in quasi-incompressible finite elasticity, International Journal for Numerical Methods in Engineering 43 (1998) 821–838.
[13] T. Yamada, Finite element procedure of initial shape determination for hyperelasticity, Structural Engineering and Mechanics 436 (1997) 173–183.
[14] V.D. Fachinotti, A. Cardona, P. Jetteur, Finite element modeling of inverse design problems in large deformations anisotropic hyperelasticity, International Journal for Numerical Methods in Engineering 74 (2008) 894–910.
[15] J. Płosa, S. Wojciech, Dynamics of systems with changing configuration and with flexible beam-like links, Mechanism and Machine Theory 35 (11) (2000) 1515–1534.
[16] P. Limaye, G. Ramu, S. Pamulapati, G.K. Ananthasuresh, A compliant mechanism kit with flexible beams and connectors along with analysis and optimal synthesis procedures, Mechanism and Machine Theory 49 (2012) 21–39.
[17] A.E. Albanesi, V.D. Fachinotti, A. Cardona, Inverse finite element method for large-displacement beams, International Journal for Numerical Methods in Engineering 84 (2010) 1166–1182.

[18] S. Kota, K.-J. Lu, Z. Kreiner, B. Trease, J. Arenas, J. Geiger, Design and application of compliant mechanisms for surgical tools, ASME Journal of Biomechanical Engineering 127 (2005) 981–989.
[19] M. Kohl, E. Just, W. Pfleging, S. Miyazaki, SMA microgripper with integrated antagonism, Sensors and Actuators 83 (2000) 208–213.
[20] V. Seidemann, S. Bütefisch, S. Büttgenbach, Fabrication and investigation of in-plane compliant SU8 structures for MEMS and their application to micro-valves and micro-grippers, Sensors and Actuators A 97–98 (2002) 457–461.
[21] A.G. Erdman, P.E. Loftness, Synthesis of linkages for cataract surgery: storage, folding and delivery of replacement intraocular lenses (IOLs), Mechanism and Machine Theory 40 (2005) 337–351.
[22] S. Timoshenko, J.N. Goodier, Theory of Elasticity, 2nd edition McGraw Hill Book Company, Inc., 1951
[23] A. Cardona, M. Géradin, A beam finite element non-linear theory with finite rotations, International Journal for Numerical Methods in Engineering 26 (1988) 2403–2438.
[24] O. Zienkiewicz, R.L. Taylor, The Finite Element Method, 5th edition, The Basis, vol. 1, Butterworth-Heinemann, 2000.
[25] O. Zienkiewicz, R.L. Taylor, The Finite Element Method, 5th edition, Solid Mechanics, vol. 2, Butterworth-Heinemann, 2000.
[26] D.B. John, W. Eaton, S. Hauberg, GNU Octave Manual Version 3, Network Theory Limited, 2008.
[27] E.L. Allgower, K. Georg, Introduction to Numerical Continuation Methods, Society for Industrial and Applied Mathematics (SIAM), 2003.
[28] H. Ren, E. Gerhard, Design and fabrication of a current-pulse-excited bistable magnetic microactuator, Sensors and Actuators A 58 (1997) 259–264.
[29] S.K. Nah, Z.W. Zhong, A microgripper using piezoelectric actuation for micro-object manipulation, Sensors and Actuators A 133 (2007) 218–224.
[30] A. Pandolfi, M. Ortiz, Improved design of low-pressure fluidic microvalves, Journal of Micromechanics and Microengineering 17 (2007) 1487–1493.